Biosynthesis of D-Alanyl-Lipoteichoic Acid: The Tertiary Structure of apo-D-Alanyl Carrier Protein[†,‡]

Brian F. Volkman,*[,§,||] Qunying Zhang,[⊥,#] Dmitri V. Debabov,[⊥,@] Edwin Rivera,[⊥,+] Gordon C. Kresheck,[○,¶] and Francis C. Neuhaus*[,⊥]

Department of Biochemistry and National Magnetic Resonance Facility at Madison, University of Wisconsin−Madison, Madison, Wisconsin 53706-1544, Department of Biochemistry, Molecular Biology and Cell Biology, Northwestern University, 2153 Sheridan Road, Evanston, Illinois 60208-3500, and Department of Chemistry, Northern Illinois University, DeKalb, Illinois 60115

Received February 20, 2001; Revised Manuscript Received April 30, 2001

ABSTRACT: The D-alanylation of lipoteichoic acid (LTA) allows the Gram-positive organism to modulate its surface charge, regulate ligand binding, and control the electromechanical properties of the cell wall. The incorporation of D-alanine into LTA requires the D-alanine:D-alanyl carrier protein ligase (AMP-forming) (Dcl) and the carrier protein (Dcp). The high-resolution solution structure of the 81-residue (8.9 kDa) Dcp has been determined by multidimensional heteronuclear NMR. An ensemble of 30 structures was calculated using the torsion angle dynamics approach of DYANA. These calculations utilized 3288 NOEs containing 1582 unique nontrivial NOE distance constraints. Superposition of residues 4−81 on the mean structure yields average atomic rmsd values of 0.43 ± 0.08 and 0.86 ± 0.09 Å for backbone and non-hydrogen atoms, respectively. The solution structure is composed of three α-helices in a bundle with additional short 3_{10}- and α-helices in intervening loops. Comparisons of the three-dimensional structure with the acyl carrier proteins involved in fatty acid, polyketide, and nonribosomal peptide syntheses support the conclusion that Dcp is a homologue in this family. While there is conservation of the three-helix bundle fold, Dcp has a higher enthalpy of unfolding and no apparent divalent metal binding site(s), features that distinguish it from the fatty acid synthase acyl carrier protein of *Escherichia coli*. This three-dimensional structure also provides insights into the D-alanine ligation site recognized by Dcl, as well as the site which may bind the poly(glycerophosphate) acceptor moiety of membrane-associated LTA.

D-Alanyl-lipoteichoic acid (D-alanyl-LTA)[1] is a macroamphiphile that plays a vital role in the growth and development of the Gram-positive organism. In many of these organisms, the hydrophilic backbone of this polymer is composed of poly(glycerophosphate) (Gro-P). The percentage of Gro-P units that are substituted with D-alanyl ester residues varies from 10 to 70% (*1*). Esterification of LTA provides a means for altering the net anionic charge of the polymer and hence of the cell wall. This macroamphiphile is postulated to influence the activities of autolysins, regulate ligand binding, and alter the electromechanical properties of the wall.

Incorporation of D-alanine into LTA requires the D-alanine:D-alanyl carrier protein ligase (AMP-forming) (Dcl) (*2*) and the D-alanyl carrier protein (Dcp) (*3*, *4*). These two proteins are encoded in the *dlt* operon together with DltB and DltD.

[†] The study was supported by NIH Grants R01 GM51621 (F.C.N.) and AI45843 (B.F.V.). For all multidimensional NMR experiments, this study made use of the National Magnetic Resonance Facility at Madison (NMRFAM), using equipment purchased with funds from the University of Wisconsin, the NSF Biological Instrumentation Program (Grant DMB-8415048), the NIH Biomedical Research Technology Program (Grant RR02301), the NSF Academic Research Instrumentation Program (Grant BIR-9214394), the NIH Shared Instrumentation Program (Grants RR02781 and RR08438), and the U.S. Department of Agriculture. Other NMR experiments were performed at the NMR Facility for Structural Biology at Northwestern University, using equipment purchased with funds provided by the W. M. Keck Foundation, the NSF (Grant DIR-8908093), and the NIH Shared Instrumentation Program (Grant RR05880). In addition, the use of the Keck Biophysics Facility at Northwestern University is acknowledged.

[‡] Coordinates for the minimized average structure and the family of 30 structures have been deposited in the RCSB Protein Data Bank as entries 1HQB and 1DV5, respectively. Chemical shifts have been deposited in the BioMagResBank under accession number 4063.

* To whom correspondence should be addressed. F.C.N.: phone, (847) 491-5656; fax, (847) 467-1380; e-mail, f-neuhaus@northwestern.edu. B.F.V.: phone, (414) 456-8400; fax, (414) 456-6510; e-mail, bvolkman@mcw.edu.

[§] University of Wisconsin−Madison.

[||] Present address: Department of Biochemistry, Medical College of Wisconsin, 8701 Watertown Plank Rd., Milwaukee, WI 53226.

[⊥] Northwestern University.

[#] Present address: Abbott Laboratories, 1401 Sheridan Rd., North Chicago, IL 60064-6256.

[@] Present address: Advanced Medicine, Inc., 901 Gateway Blvd., South San Francisco, CA 94080.

[+] Present address: Department of Medicinal Chemistry and Molecular Pharmacology, 1333 RHPH Building, Purdue University, West Lafayette, IN 47907.

[○] Northern Illinois University.

[¶] Present address: Department of Chemistry, University of Colorado at Colorado Springs, Colorado Springs, CO 80933-7150.

[1] Abbreviations: Dcp, D-alanyl carrier protein; Dcl, D-alanine:Dcp ligase (AMP-forming); LTA, lipoteichoic acid; ACP, acyl carrier protein; HSQC, heteronuclear single-quantum coherence; NOESY, nuclear Overhauser effect spectroscopy; DSC, differential scanning calorimetry; CD, circular dichroism; TAD, torsion angle dynamics; rmsd, root-mean-square deviation; AcpP, *E. coli* fatty acid synthase ACP; act ACP, *S. coelicolor* actinorhodin polyketide synthase ACP; PCP, *B. brevis* nonribosomal peptide synthetase peptidyl carrier protein domain; 2D, two-dimensional; 3D, three-dimensional.

10.1021/bi010355a CCC: $20.00
Published on Web 06/14/2001

Dcp provides an essential link between the ligase and the incorporation of D-alanine into LTA. The gene that encodes this carrier protein, designated *dltC*, has been characterized in *Lactobacillus rhamnosus* (previously designated *Lactobacillus casei*) ATCC 7469 (*3*, *4*) and *Bacillus subtilis* (*5*, *6*). DltD functions in the selection of the correct carrier protein (Dcp) for ligation and in the hydrolysis of mischarged D-alanyl-ACPs (*7*).

We have hypothesized that Dcp is a homologue of the acyl carrier protein (ACP) involved in fatty acid biosynthesis (*3*). This was based on (i) the ability of apo-Dcp to be processed by holo-ACP synthase, (ii) the ability of Dcp and ACPs to be ligated with D-alanine in the reaction catalyzed by Dcl, (iii) amino acid similarity around the phosphopantetheine attachment site, and (iv) the similarity of the predicted secondary structure to that established for AcpP. The goal of this study was to determine the structure of Dcp and compare it with structures of ACPs involved in fatty acid and antibiotic biosyntheses. Structures are currently available for *Escherichia coli* AcpP (*8*−*10*), the apo form of *Streptomyces coelicolor* actinorhodin polyketide synthase ACP (act apo-ACP) (*11*), and peptidyl carrier protein (PCP) of the nonribosomal peptide synthetase from *Bacillus brevis* (*12*). Because the prosthetic group has no effect on the NMR spectrum of AcpP (*13*), apo-Dcp was chosen for this study.

Here, we report the complete ^{1}H, ^{13}C, and ^{15}N resonance assignments and high-resolution solution structure of apo-Dcp. Comparison of this structure with ACPs of known structure confirms the relationship suspected from sequence analysis (*3*). This structure provides the basis for defining the specificity determinants which function for D-alanine incorporation into LTA.

MATERIALS AND METHODS

Chemicals and Protein Production. Growth media, Martek 9-N, Celtone-CN, and [99% U-^{13}C]glucose were purchased from Martek Biosciences. $^{15}NH_4Cl$ was purchased from ICN Biomedicals. *E. coli* strain BL21(DE3) was obtained from Novagen. Plasmid pDCP1 containing the gene for apo-Dcp was constructed as described previously (*3*). Recombinant apo-AcpP (*14*) from *E. coli* was a gift of R. Flugel and C. Walsh. The preparation of unlabeled apo-Dcp using pDCP1 was as described by Debabov et al. (*3*).

Preparation of Labeled Protein Samples. We previously described the expression of *L. rhamnosus* Dcp in *E. coli* (*3*), and have now used this overexpression system to produce uniformly ^{13}C- and ^{15}N-labeled apo-Dcp for structural analysis by NMR. For the preparation of [U-^{15}N]apo-Dcp, *E. coli* BL21(DE3) cells containing pDCP1 were grown in Martek 9-N medium (1 L) with 100 mg/L ampicillin at 37 °C. The culture was induced at an OD_{600} of 0.4 with 0.4 mM IPTG. Cells were harvested by centrifugation 4 h after induction and lysed by freezing and thawing as described previously (*3*). Apo-Dcp was isolated in pure form by bulk adsorption to DEAE-cellulose pre-equilibrated in 70 mM bis-Tris (pH 6.5) and 100 mM NaCl and eluted with 70 mM bis-Tris (pH 6.5) and 600 mM NaCl. Additional purification was achieved by preparative native PAGE as described previously (*3*). The molecular mass of the purified protein was 8884 Da, as determined by electrospray mass spectrometry, performed on a VG Quattro (Fisons Instruments) triple-quadrupole mass spectrometer equipped with an electrospray ion source. This mass value corresponded to a level of ^{15}N incorporation of >94%. The [U-^{15}N,^{13}C]apo-Dcp was prepared with pDCP1 in BL21(DE3) cells grown in M9 medium (*15*) containing 20% Celtone-CN, 1% ^{13}C-labeled glucose, and 1% ^{15}N-labeled NH_4Cl. All other conditions for growth, induction, and isolation of [U-^{15}N,^{13}C]apo-Dcp were the same as for [U-^{15}N]apo-Dcp.

Differential Scanning Calorimetry. Calorimetric measurements were performed with the VP-DSC MicroCalorimeter (MicroCal Inc., Northampton, MA) with a scanning rate of 1.0 °C/min. An appropriate baseline was obtained that reflected the heat capacity difference before and after the transition. The van't Hoff enthalpy change for the thermal transition was given by the expression (*16*)

$$\Delta H_{vH} = AR(T_{1/2})^2(c_{ex,1/2}/\Delta H_{cal})$$

where ΔH_{cal} is the calorimetric specific enthalpy, $T_{1/2} = t_{1/2} + 273.15$, $t_{1/2}$ is the temperature (°C) at which the process is half-completed, and $c_{ex,1/2}$ is the excess specific heat at $t_{1/2}$. R is the gas constant, and the factor A has a value of 4.00 for a simple two-state transition. Samples of apo-Dcp were dialyzed against 50 mM NaAc (pH 6.1), and the dialysate was used in the reference cell.

Circular Dichroism. Thermally induced denaturation of either 0.18 mM apo-Dcp or apo-AcpP was monitored by circular dichroism (CD) performed in a 0.2 mm cell at 222 nm. A model J-715 spectropolarimeter (Jasco, Inc.) equipped with an RTE-3 refrigerated/heater circulator (Neslab Instruments, Inc.) was used.

NMR. Thermally induced denaturation of apo-Dcp in 99% D_2O was monitored by ^{1}H NMR on a Bruker AMX600 instrument at the NMR Facility for Structural Biology at Northwestern University. All multidimensional NMR experiments were carried out at 25 °C on a Bruker DMX600 spectrometer equipped with a 5 mm triple-resonance ^{1}H/^{15}N/^{13}C probe and three-axis pulsed field gradients at the National Magnetic Resonance Facility at Madison (NMRFAM). NMR samples contained either 1.2 mM [^{15}N]apo-Dcp or 1.8 mM [^{15}N,^{13}C]apo-Dcp in 50 mM potassium phosphate buffer (pH 5.8), containing a 90% H_2O/10% D_2O mixture.

Most pulse sequences incorporated sensitivity enhancement (SE) with magic angle (*17*, *18*) gradient coherence selection and a flip-back scheme to preserve signal intensity for exchangeable amide resonances (*19*). For non-SE experiments, water suppression was achieved with the WATERGATE method incorporating a 3-9-19 selective inversion pulse. Quadrature detection in the indirectly detected dimensions was obtained by the States−TPPI method (*20*). All resonance assignments and distance constraints were derived from the following experiments: 3D ^{15}N SE NOESY-HSQC (*21*), 3D ^{15}N SE TOCSY-HSQC (*21*), 2D ^{15}N-filtered NOESY (*22*), 3D SE HNCACB (*23*−*25*), 3D HCCH-TOCSY (*26*), 3D SE C(CO)NH (*27*), 3D SE HNCA (*19*, *24*, *28*), 3D SE HNCO (*24*, *28*), 3D SE HCACO (*29*, *30*), ^{15}N-edited HSQC (*31*), 3D HNHA (*32*, *33*), 3D HNHB (*34*), 3D ^{13}C SE NOESY-HSQC (one each for the aromatic and aliphatic ^{13}C regions), and ^{13}C constant-time SE HSQC (*35*). All NOESY mixing times were 80 ms. Isotropic mixing periods were 22 ms (CCONH) and 60 ms (^{15}N TOCSY-HSQC).

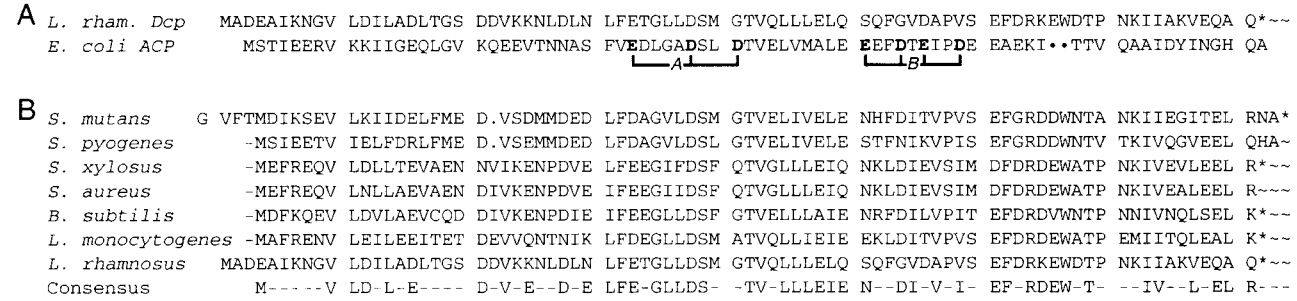

FIGURE 1: (A) Alignment of the sequences of AcpP and Dcp. The Ca^{2+} binding residues of AcpP are shown in bold, and the two putative ligand binding sites (A and B) are indicated. (B) Multiple alignment of Dcps from various species with highly conserved residues shown at the bottom.

All data were processed with either Felix95 (Molecular Simulations) or NMRPipe (*36*). Chemical shifts were referenced to internal DSS (2,2-dimethyl-2-silapentane-5-sulfonate) as 0 ppm (^{1}H) and indirectly for ^{15}N and ^{13}C using the following ratios: 0.251449530 for ^{13}C/^{1}H and 0.101329118 for ^{15}N/^{1}H (*37*). Complete resonance assignments were obtained using Felix95, XEASY (*38*), and Sparky. The consensus chemical shift index was calculated from the assigned $^1H^{\alpha}$, $^{13}C^{\alpha}$, $^{13}C^{\beta}$, and $^{13}C'$ shifts using the CSI program (*39*, *40*).

Structure Determination. Assignments of NOEs were obtained manually using XEASY (*38*) and automatically using DYANA 1.5 (*41*). Structures were calculated with the torsion angle dynamics approach of DYANA 1.5 using 4000 steps per structure in the early stages of refinement, and 8000 steps in the final round, followed in each case by 1000 steps of conjugate gradient minimization. Distance constraint upper bounds were generated with the CALIBA function of DYANA. For the initial rounds of structure calculations, manually assigned additional NOEs were used as input restraints. Each round started with 20 random conformers, from which the 10 with the lowest target function were used to analyze constraint violations and assign additional NOE constraints in DYANA for the following round of refinement. This process was repeated until more than 90% of the cross-peaks in the 3D spectra had been assigned and all consistent violations were eliminated. In the final round of refinement, a total of 50 structures were calculated and the 30 conformers with the lowest target function were considered for analysis. The mean structure calculated in MOLMOL (*42*) from this ensemble of 30 structures was minimized in DYANA with 1000 steps of conjugate gradient minimization and reported as the representative apo-Dcp structure. All subsequent analyses of the structure were performed using DYANA, MOLMOL, and PROCHECK-NMR (*43*).

RESULTS

Thermally Induced Denaturation of Apo-Dcp in the Presence of Ca^{2+} As Measured by NMR, DSC, and CD. The structural analysis of apo-Dcp was led by previous results from Prestegard and co-workers on *E. coli* AcpP (*8*−*10*). While the extent of sequence identity between these proteins is low (20%), as shown in Figure 1A, it was proposed that Dcp is an ACP homologue likely to have similar features of secondary and tertiary structure (*3*). In the structural studies of AcpP, Horvath et al. (*44*) found that the addition of Ca^{2+} stabilized the protein to thermal denaturation. AcpP has two divalent metal ion binding sites (Figure 1A) (*45*−*47*). With the goal of stabilizing a single conformer, the NMR analysis of the AcpP solution structure included the addition of Ca^{2+}. Thus, in the initiation of our structural studies of Dcp, it was important to establish whether Ca^{2+} binding might also affect the thermal denaturation of the protein and hence determine the conformational stability of Dcp.

To examine the role that Ca^{2+} plays in stabilizing the structure, thermal denaturation of apo-Dcp was examined by ^{1}H NMR. Two series of spectra were collected with samples of apo-Dcp prepared identically except for the addition of 10 mM Ca^{2+} to one sample. Portions of the spectra containing the aromatic signals of residues Trp^{67}, Phe^{32}, Phe^{53}, and Phe^{62} and the $^1H^{\alpha}$ resonance of Thr^{69} are shown in Figure 2 as a function of increasing temperature. Comparison of the two spectra from 25 to 50 °C revealed no obvious indication of Ca^{2+} binding by apo-Dcp. At >55 °C, thermal unfolding (broadening, shifting of resonances) was observed for both samples, but again no detectable differences as a function of Ca^{2+} were detected.

Differential scanning calorimetry (DSC) provided another method for assessing the $t_{1/2}$ for unfolding (*16*, *48*). The $t_{1/2}$ for apo-Dcp is 68.99 ± 0.06 °C with a ΔH_{vH} of 56.5 ± 0.2 kcal/mol when measured in 50 mM NaAc (pH 6.1). The addition of 10 mM Ca^{2+} gave a $t_{1/2}$ of 70.76 ± 0.16 °C and a ΔH_{vH} of 60.4 ± 0.05 kcal/mol. The agreement of ΔH_{cal} (57.0 ± 0.1 and 61.2 ± 0.04 kcal/mol, respectively) with ΔH_{vH} in the absence and presence of cation is consistent with the assumed two-state unfolding process. In contrast, $t_{1/2}$ and ΔH_{vH} for AcpP are 52.7 °C and 40.8 kcal/mol in 50 mM NaAc (pH 6.1) (low salt) in the absence of Ca^{2+} (*44*). In the presence of 8.3 mM Ca^{2+} (low salt), $t_{1/2}$ increased to 64.3 °C and ΔH_{vH} increased to 55.3 kcal/mol. The observations with apo-Dcp reflect an intrinsic heat stability that is higher than that of AcpP and suggest that Dcp does not show an increased level of stabilization in the presence of Ca^{2+}.

To examine further the differences in stability between AcpP and Dcp, thermally induced denaturation was monitored by CD for each protein in the presence and absence of Ca^{2+}. The $t_{1/2}$ of apo-AcpP was 51.4 °C when measured in 10 mM NaAc (pH 6.1). In contrast, under identical conditions, the $t_{1/2}$ of apo-Dcp was 65.0 °C. The addition of 10 mM $CaCl_2$ to apo-AcpP and apo-Dcp resulted in an increase in $t_{1/2}$ to 60.0 and 65.8 °C, respectively. The differences in Ca^{2+} stabilization as measured by $t_{1/2}$ (0.8 °C for apo-Dcp and 8.6 °C for apo-AcpP) support the conclusion that apo-Dcp is intrinsically more stable than apo-AcpP. In contrast

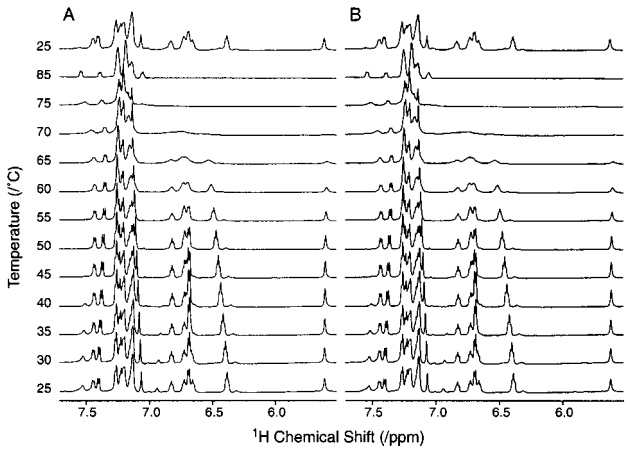

FIGURE 2: Temperature titration of the aromatic ^{1}H signals of apo-Dcp in the (A) presence and (B) absence of 10 mM Ca^{2+} at 600 MHz. One-dimensional ^{1}H spectra were acquired for the unlabeled protein in 99% D_2O as a function of increasing temperature. The uppermost spectrum, acquired after cooling from 85 to 25 °C, demonstrates the reversibility of thermal denaturation for apo-Dcp.

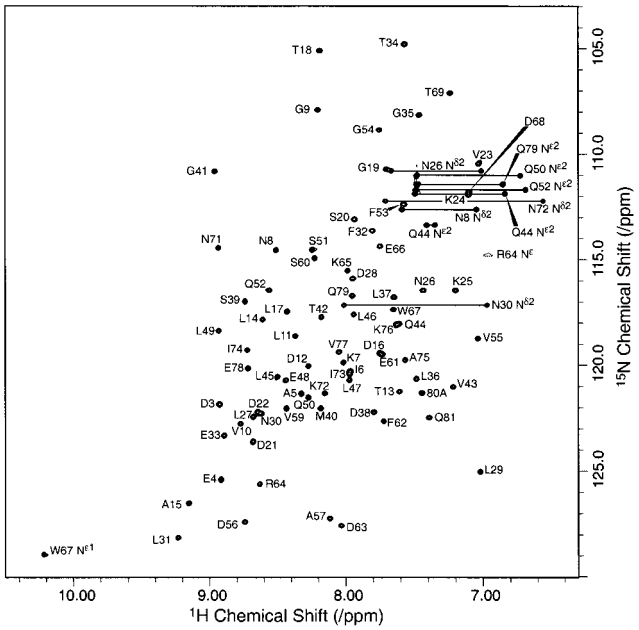

FIGURE 3: 2D ^{1}H−^{15}N HSQC spectrum of [U-^{15}N]apo-Dcp at 600 MHz and 25 °C. Backbone amide signals are labeled with the one-letter amino acid code and residue number. Side chain amide NH_2 resonances are connected with horizontal lines and labeled. The cross-peak for Arg^{64} H$^{\epsilon}$ is aliased from a ^{15}N chemical shift of 84.9 ppm.

to apo-AcpP, the addition of Ca^{2+} to apo-Dcp in either DSC or CD had essentially no effect in the thermally induced denaturation.

The conditions for the measurements given above, 50 mM NaAc (pH 6.1), were chosen on the basis of those conditions used by Prestegard and co-workers for the NMR structural analysis of AcpP (*8*−*10*). When apo-AcpP and apo-Dcp were compared in CD experiments using 10 mM phosphate buffer (pH 7.0), the results also revealed a large difference in $t_{1/2}$ for the two proteins (31.8 °C for apo-AcpP and 58.7 °C for apo-Dcp). Thus, while the intrinsic stability of both proteins decreased, the $t_{1/2}$ for apo-Dcp is 26.9 °C higher than that of apo-AcpP at pH 7.

Absence of Ca^{2+} Binding Sites in Apo-Dcp. Since Ca^{2+} increased the stability of AcpP in thermally induced denaturation as measured by both DSC and CD, it was important to determine whether Dcp has the putative cation binding sites similar to those detected in AcpP. Frederick et al. (*45*) located the divalent ion binding sites in AcpP using relaxation-perturbed 2D NMR. The acidic residues serving as coordinating ligands are identified in Figure 1A. An alignment of seven Dcp sequences in Figure 1B shows that only two of the three coordinating ligands from site A are conserved, corresponding to Glu^{33} and Asp^{38}. Only the second of four acidic side chains in site B is conserved in the Dcp family, but in *L. rhamnosus*, this residue is a glycine (Gly^{54}). Thus, it would appear from these alignments and the results from NMR (Figure 2), DSC, and CD that Dcp lacks the Ca^{2+} binding sites detected in AcpP. On the basis of these results, Ca^{2+} was not included in the samples for NMR structural analysis of apo-Dcp.

Resonance Assignments. The ^{1}H−^{15}N HSQC spectrum of ^{15}N-labeled apo-Dcp is shown in Figure 3. In this spectrum, 77 expected correlation peaks for the backbone amide resonances were assigned. The spectrum also shows 20 additional peaks from asparagine (8), glutamine (10), tryptophan (1), and arginine (1) side chain resonances. Backbone assignments were made primarily on the basis of the HNCACB and C(CO)NH spectra, with the use of HNCA, HNCO, and HCACO data to resolve ambiguities. Sequential assignments were further verified with the analysis of the 3D ^{15}N NOESY-HSQC spectrum. Aliphatic side chains were assigned using ^{15}N TOCSY-HSQC, CCONH, and HCCH-TOCSY data. Aromatic side chain assignments were deduced from 2D ^{15}N-filtered NOESY and ^{13}C−^{1}H HSQC spectra on the basis of NOEs to the $^1H^{\alpha}$ and $^1H^{\beta}$ resonances of those amino acids.

A few distinctive features were noted in the chemical shift assignments for apo-Dcp. For example, all side chain ^{1}H signals of Lys^{76} are located far upfield of their random-coil values. Chemical shift values of 0.96 and −0.36 ppm were observed for the Lys^{761} $^1H^{\gamma}$ resonances. This may be the result of ring-current effects from Trp^{67}. Hydroxyl protons, normally broadened beyond detection by exchange with solvent water, were observed for the side chains of Thr^{18} (4.48 ppm) and Thr^{69} (5.79 ppm). These two exchangeable ^{1}H signals exhibited neither one-bond scalar couplings to ^{15}N or ^{13}C nor correlations in the ^{15}N TOCSY-HSQC spectra. As apo-Dcp contains no cysteine, a hydroxyl proton was presumed to be the remaining assignment possibility in each case. Sequence-specific resonance assignments were deduced from strong intraresidue NOEs to both the other side chain and backbone protons. Detection of the exchangeable Thr^{18} and Thr^{69} $H^{\gamma 1}$ resonances predicts low solvent accessibilities or side chain hydrogen bonding interactions for these residues, as discussed below. Except for aromatic $^{13}C^{\gamma}$ and side chain carbonyl ^{13}C resonances, assignments were obtained for all ^{1}H, ^{15}N, and ^{13}C chemical shifts of apo-Dcp, and are available from the BioMagResBank (BMRB accession number 4063).

Chemical Shift and NOE Analysis of Secondary Structure. Figure 4 summarizes short- and medium-range NOEs for apo-Dcp, as well as the consensus chemical shift index (CSI) determined from $^1H^{\alpha}$, $^{13}C^{\alpha}$, $^{13}C^{\beta}$, and $^{13}C'$ shifts. Three major helical regions were identified. Though not predicted by the consensus CSI, which requires a continuous pattern of helical

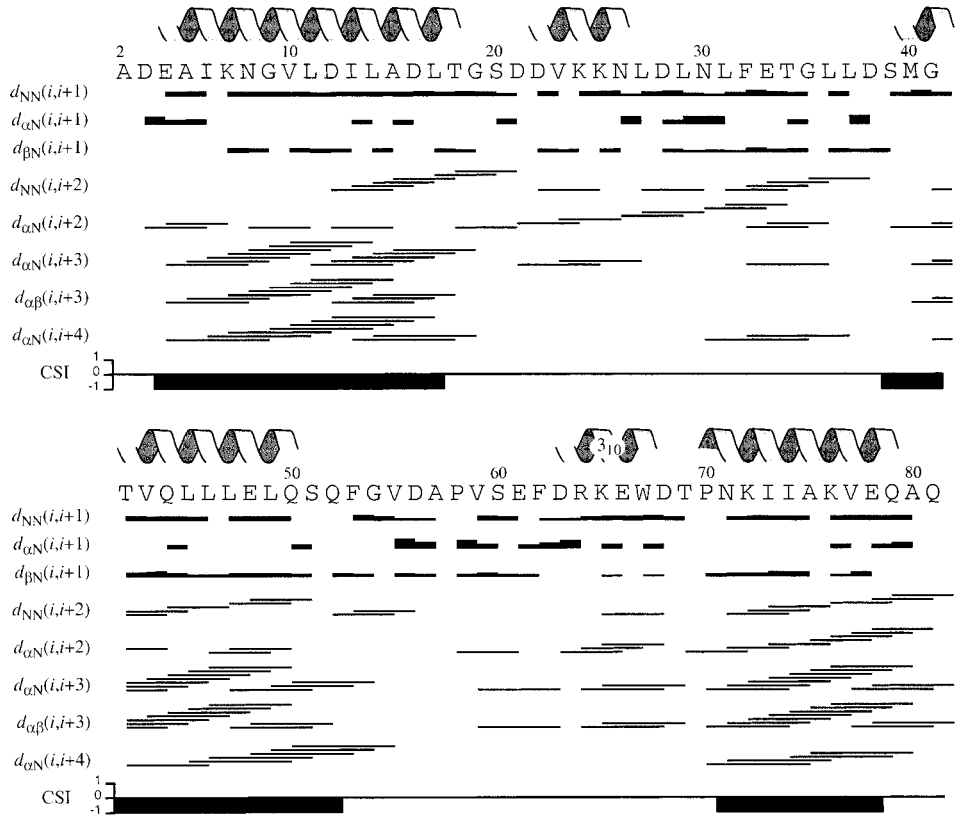

FIGURE 4: Summary of sequential and medium-range NOE patterns and chemical shift index (CSI) for apo-Dcp. The sequence is shown starting with Ala[2], since the amino-terminal Met is absent. The relative intensity of sequential NOEs is indicated by the height of the connecting box. Horizontal lines indicate the observation of medium-range NOEs between residue pairs. The consensus CSI obtained from $^1H^\alpha$, $^{13}C^\alpha$, $^{13}C^\beta$, and $^{13}C'$ chemical shifts is shown, with values of +1, 0, and −1 indicating sheet, coil, and helix, respectively. Helical regions of apo-Dcp, as defined by backbone geometry and hydrogen bonds observed in the calculated structures, are indicated above the amino acid sequence.

shifts for at least four residues, two short helices, I′ and II′, are suggested by patterns of (i, $i + 2$) and (i, $i + 3$) NOEs.

Three-Dimensional Structure Determination. From a total of 3288 assigned NOEs in four different NOESY spectra, 1582 unique nontrivial NOE upper limit distance constraints were generated with the CALIBA function in DYANA. The distributions of constraints by range and by sequence position are summarized in Table 1 and Figure 5A, respectively. No other types of experimental constraints were included in any of the DYANA TAD calculations. The ensemble of 30 TAD structures resulting from the final stage of refinement is shown in Figure 6A. Good agreement with the experimental restraints is reflected in the low DYANA target functions (0.68 ± 0.11 Å^2) obtained for the family of structures. Superposition of residues 4−81 on the mean structure yields rmsd values of 0.43 ± 0.08 and 0.86 ± 0.09 Å for backbone atoms and non-hydrogen atoms, respectively. The rmsd values for each residue are plotted in Figure 5B. Only amino-terminal residues Ala[2] and Asp[3] are significantly disordered. Another measure of structure quality is provided by Ramachandran analysis of the ensemble, which places 73.8% of the residues in the most favored regions, 23.4% in additional allowed regions, 2.6% in generously allowed regions, and only 0.2% in disallowed regions. To provide a representative conformer with normal covalent geometry, the mean structure was minimized in DYANA to a final target function of 0.82 Å^2. Structural statistics for the family and the refined average structure are summarized in Table 1.

Hydrogen Bonding. The family of structures was analyzed for frequently occurring hydrogen bonding interactions. Though only NOE restraints were included in the structure calculations, good backbone hydrogen bonding geometry (H-bond length < 2.4 Å, angle < 35°) was observed throughout each of the helical regions of apo-Dcp. Residues Glu[4]−Gly[19], Met[40]−Leu[49], and Pro[70]−Gln[79] comprise the three major α-helices as indicated by patterns of (i, $i + 4$) hydrogen bonds. A single turn of α-helix is suggested by the H-bond between Asp[22] O and Asn[26] H^N, and the (i, $i + 3$) H-bond between Asp[63] and Glu[66] is consistent with the formation of a short 3_{10}-helix. The combination of hydrogen bond patterns and Ramachandran analysis of backbone geometry provides a consensus for the location of secondary structure elements in apo-Dcp (Figure 4). Additional main chain−main chain hydrogen bonds include the long-range interaction between Leu[31] H^N and Asp[68] O, a type I reverse turn closed by the Phe[32] O−Gly[35] H^N hydrogen bond, and H-bonds between Leu[31] O and Leu[37] H^N and between Leu[49] O and Val[55] H^N. One side chain−main chain hydrogen bond is also observed between Thr[18] $O^{\gamma 1}$ and Ser[20] H^N. An NOE between the Thr[18] $H^{\gamma 1}$ and Ser[20] H^N protons provides additional evidence for this interaction. While NOEs from the Thr[69] hydroxyl to a number of other residues are observed (Asp[28], Asn[71], and Lys[72]), no specific hydrogen bond was observed in the family of structures.

Hydrophobic Core Interactions. The tertiary structure of apo-Dcp is stabilized by numerous hydrophobic interactions.

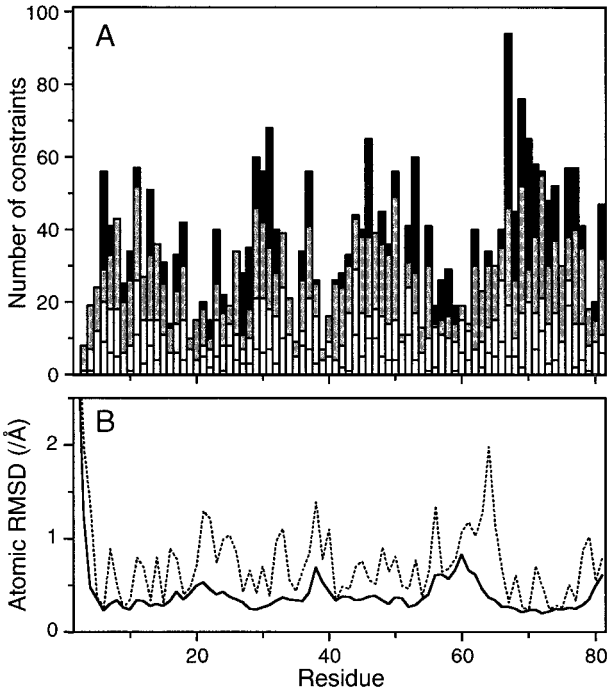

FIGURE 5: Restraint density and local coordinate precision for the NMR structure of apo-Dcp. (A) Distribution by residue of NOE constraints used in the structure determination of apo-Dcp. For each residue, the numbers of intraresidue, sequential, medium-range ($1 < |i - j| < 4$), and long-range NOEs are shown with white, light gray, dark gray, and black bars, respectively. (B) Plots of N, C^{α}, and C′ (solid line) and all non-hydrogen (dotted line) average atomic rmsd values for each residue. Coordinates were superimposed on the mean structure using residues 4−81. The rmsd values for the N-terminal residue, Ala[2], are 3.61 Å (N, C^{α}, and C′) and 3.53 Å (non-hydrogen).

Table 1: Structural Statistics for 30 Apo-Dcp Conformers[a]

type of NOE constraint	no.
long	332
medium	560
short	372
intraresidue	318
total	1582
constraints/residue	19.8

DYANA parameters	⟨TAD⟩	⟨TAD⟩$_r$
target function (Å^2)	0.68 ± 0.11	0.82
upper limit violations		
no. >0.1 Å	14 ± 3	11
sum of violations (Å)	5.5 ± 0.7	5.6
maximum violation (Å)	0.22 ± 0.04	0.19
van der Waals violations		
no. >0.1 Å	1 ± 1	4
sum of violations (Å)	2.3 ± 0.3	3.3
maximum violation (Å)	0.12 ± 0.04	0.15

average atomic rmsds (Å)[b]	$\overline{\langle TAD \rangle}$	⟨TAD⟩$_r$
N, C^{α}, C′	0.43 ± 0.08	0.50 ± 0.08
all non-H	0.86 ± 0.09	1.08 ± 0.12

[a] ⟨TAD⟩, ensemble of 30 DYANA TAD conformers; $\overline{\langle TAD \rangle}$, average coordinates obtained from a least-squares superposition of residues 4−81; $\overline{\langle TAD \rangle}_r$, representative structure obtained by applying 1000 steps of conjugate gradient minimization to the mean structure, $\overline{\langle TAD \rangle}$. [b] Average atomic rmsds were calculated by superposition of either backbone N, C^{α}, and C′ atoms or all non-hydrogen atoms of ⟨*TAD*⟩ vs $\overline{\langle TAD \rangle}$ and ⟨*TAD*⟩ vs ⟨TAD⟩$_r$ using residues 4−81.

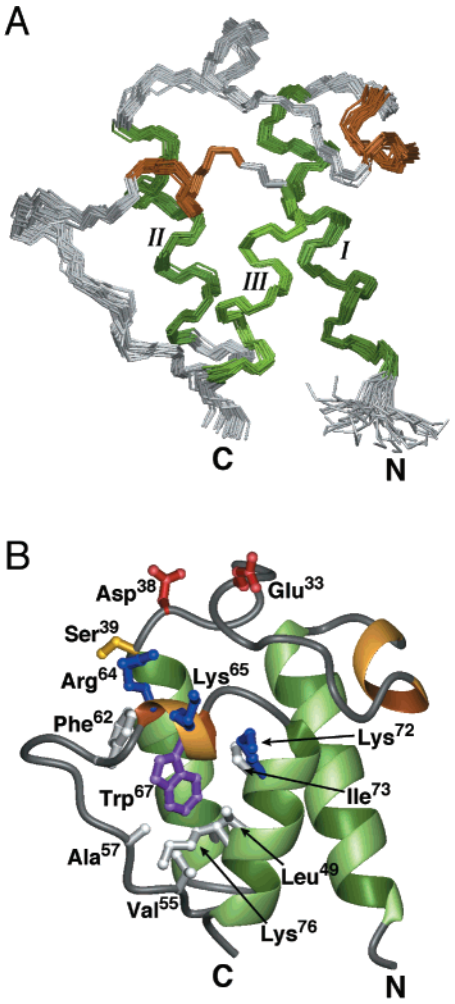

FIGURE 6: NMR structure of apo-Dcp. (A) Ensemble of 30 apo-Dcp torsion angle dynamics conformers (PDB entry 1DV5) after alignment of the backbone atoms of residues 4−81. The backbone N, C^{α}, and C′ atoms are shown, with the three major α-helices (I, residues 4−18; II, residues 40−49; and III, residues 70−79) colored green, short intervening helices orange, and all other residues gray. (B) Ribbon diagram of the minimized average structure of apo-Dcp (PDB entry 1HQB) with a number of key side chains displayed and labeled. Residues shown in white bury the Trp[67] side chain (purple) in the hydrophobic core. Other key residues include the conserved Glu[33] and Asp[38] (red) and Ser[39] (yellow) as well as a cluster of basic residues (blue) proximal to the phosphopantetheine attachment site (Arg[64], Lys[65], and Lys[72]).

Apolar side chains with less than 24% of their surface area accessible to solvent include Val[10], Leu[14], Val[23], Leu[31], Leu[45], Leu[49], Phe[53], Val[55], Ala[57], Trp[67], Pro[70], Ile[73], Ile[74], and Val[77]. Most of these residues have heavy atom rmsds below 0.5 Å [Figure 5B (dotted line)]. This represents residues from all three major helices and the two minor helices, as well as residues from the extended regions preceding and following helix II. The Trp[67] side chain, a unique feature of all Dcp sequences (Figure 1B), is involved in the hydrophobic stabilization of the apo-Dcp structure (Figure 6B). This side chain has close contacts to Leu[49], Val[55], Ala[57], Phe[62], Ile[73], and Lys[76], resulting in 89% of its surface area being buried in the core of the protein.

Helix Topology and Charge Distribution. Helix I is arranged in an antiparallel orientation relative to helices II and III, matching the topology of the three-helix bundle characteristic of the ACP family. Helix II has a higher content

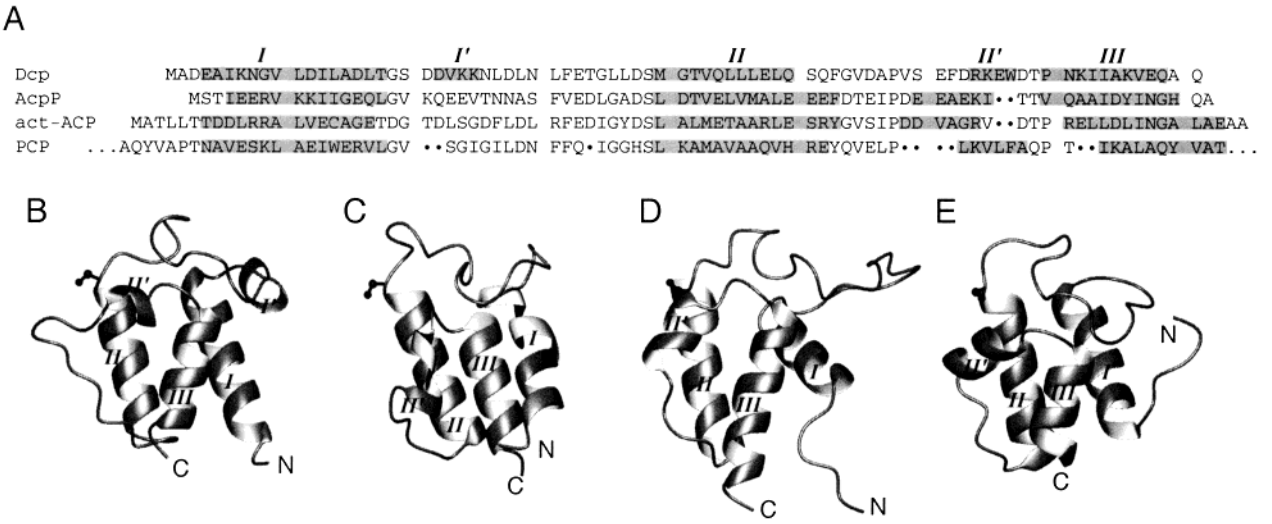

FIGURE 7: Comparison of ACP structures with apo-Dcp NMR structure. (A) Sequences of ACPs for which three-dimensional structures are available (helices are labeled and shaded). (B−E) Comparison of the apo-Dcp structure with three ACPs. Each was superimposed on the minimized average apo-Dcp structure (B) using backbone (N, C^{α}, and C′) atoms of the specified residues of Dcp and is shown in the same orientation. (C) AcpP (PDB entry 1ACP, model 1) was superimposed using residues 5−17, 39−52, and 71−79, with a resulting backbone rmsd of 2.1 Å. (D) act ACP (PDB entry 2AF8) was superimposed using residues 5−15, 39−53, and 68−81, with a resulting backbone rmsd of 2.0 Å. (E) PCP (PDB entry 1DNY, model 1) was superimposed using residues 5−17, 39−52, and 74−81, with a resulting backbone rmsd of 1.7 Å. The conserved serine which serves as the site of phosphopantetheine attachment is shown for each protein.

of hydrophobic residues than the other more amphipathic helices (Figure 4). Examination of the structure reveals that side chains of Met^{40}, Val^{43}, and Leu^{47} are exposed to solvent. The face of helix II combines with loop residues Pro^{58}, Val^{59}, and Phe^{62} to form a hydrophobic cleft adjacent to Ser^{39}, the attachment site for phosphopantetheine. Dcp is an acidic protein (pI 3.98) (*3*) whose surface charge is dominated by 10 Asp and 6 Glu side chains. Two conserved acidic residues, Glu^{33} and Asp^{38} (Figure 1B), correspond to Ca^{2+}-binding ligands in AcpP. On the basis of their relative orientation (Figure 6B), these side chains are unlikely to contribute to a metal binding site. The seven positive charges from one Arg and six Lys residues are also solvent-exposed. Three of them, Arg^{64}, Lys^{65}, and Lys^{72}, cluster in proximity to Ser^{39}.

DISCUSSION

Although the sequences of Dcp and AcpP are only 20% identical, it was proposed that Dcp is a homologue of the carrier protein involved in fatty acid biosynthesis (*3*). The determination of the three-dimensional solution structure of apo-Dcp provides the features of secondary and tertiary structure for comparison with AcpP, act ACP, and PCP, as shown in Figure 7. The three-helix bundle fold of these proteins is also maintained in apo-Dcp, and thus, Dcp is a true conformational homologue of AcpP, act ACP involved in polyketide synthesis, and PCP involved in nonribosomal peptide synthesis.

Comparison of Apo-Dcp with Other ACP Structures. For purposes of comparison, we will refer to the three major helices as I, II, and III. While Dcp and the other known ACP structures all share the conserved three-helix bundle fold, there are notable differences. In Figure 7, the apo-Dcp minimized average structure (Figure 7B) is compared with AcpP (Figure 7C), act ACP (Figure 7D), and PCP (Figure 7E). Helix orientations in apo-Dcp and PCP are similar, within ∼10° of each other. Helix III in AcpP (Figure 7C) and helix I in act ACP (Figure 7D) are tilted ∼30° compared to those in apo-Dcp. In addition, the lengths of helices I and III vary among the structures, with a shorter helix I and longer helix III in act ACP. The first turn of helix III is missing in PCP when compared to the others. The length and orientation of helix II are the most consistent structural elements of the ACP family. These may reflect a role in preserving recognition associated with the conserved phosphopantetheine attachment site.

In addition to the comparisons made in Figure 7, features of the nodulation protein (NodF) have also been compared to those of Dcp. NodF is an ACP whose sequence is 27% identical to that of AcpP. It contains the three-helix bundle fold characteristic of this family (*49*). However, AcpP cannot functionally replace NodF in an in vivo assay (*50*). Thus, while the conformational structure of AcpP is similar to that of the NodF protein, there are recognition elements that define its function. While the coordinates of the NodF solution structure have not been published (*49*), it is apparent that the tertiary fold of apo-Dcp is similar. This is a particularly interesting comparison because a functional analysis of this protein using an ACP chimera has defined a target recognition site in the C-terminal region (*50*). A similar analysis with Dcp may also provide a definition of the recognition sites described below.

The apo-Dcp structure contains two short helices, I′ and II′, in the loop regions connecting helices I and II and helices II and III. While all four proteins show evidence of a helix II′, helix I′ is found only in the Dcp structure. Helix II′ is not consistently positioned in the structural comparisons, and inspection of the aligned sequences (Figure 7A) shows that the location and lengths of this helix and its connecting loops are variable. The 3_{10}-helix in apo-Dcp spans residues Asp^{63}−Trp^{67} and may be similar in orientation to the corresponding helix of PCP. Trp^{67} is only 11% solvent accessible, and thus, the hydrophobic interactions with this residue may play a significant role in the intrinsic thermal stability of Dcp while helping to position a highly conserved Arg^{64}.

It was hypothesized by Kim and Prestegard (*51*) that *E. coli* AcpP consists of two conformers in dynamic equilibrium. Backbone amide protons in helix II were found to exchange more rapidly than those in helices I and III. The instability in helix II may be responsible for the mobility between the two conformers. Since AcpP has to interact with at least six different enzymes in fatty acid biosynthesis, a measure of conformational flexibility may be necessary for functional diversity. As confirmed in this paper, AcpP is stabilized by divalent cations, e.g., Ca^{2+}. The metal ligand may also play structural roles that are required for protein function. Neither the dynamic conformational equilibrium nor the stabilization by Ca^{2+} seen for AcpP was observed with apo-Dcp. Apo-Dcp is intrinsically more stable to unfolding than apo-AcpP. Moreover, the addition of divalent metal cations to apo-Dcp does not result in higher thermal transitions. Thus, these features distinguish Dcp from the AcpP involved in fatty acid biosynthesis. Structural NMR studies of act ACP and PCP also did not reveal any evidence of large-scale conformational heterogeneity, suggesting that in terms of thermal stability these proteins may be more like Dcp than AcpP.

D-Alanine Ligation Site. The ligation of D-alanine to Dcp requires the recognition of the phosphopantetheine prosthetic group by Dcl. However, not only does Dcl recognize the prosthetic group on Dcp, but the enzyme also recognizes the group in all ACPs which have been tested (*4*, *52*). The structural comparisons in Figure 7 illustrate the degree to which the location of the serine residue for the attachment of this prosthetic group is conserved in the ACP family. In addition, sequence alignments show good similarity immediately before and after the conserved serine. Since Dcl would appear to have a low specificity for ligating D-alanine to the carrier protein, other mechanisms are required to avoid mischarging ACPs with D-alanine. For Dcp, this function is performed by DltD together with Dcl and Dcp (*7*). Thus, the complex of these proteins ensures that the correct carrier protein is ligated with D-alanine.

Putative Poly(Gro-P) Binding Surface. Only D-alanyl-Dcp donates its activated D-alanine to the poly(Gro-P) moiety of LTA (*4*, *52*), and thus, it was proposed that Dcp has a binding site for LTA which is not found in the ACPs involved in fatty acid synthesis and metabolism. In addition, Kiriukhin and Neuhaus (*53*) observed that the incubation of D-alanyl-Dcp with highly purified LTA results in the hydrolysis of the D-alanyl thioester. A critically positioned positive residue that may play a role in the electrostatic interaction with a phosphodiester linkage of LTA is Arg^{64}. It is located in the RKEWD motif (Figure 1B) found in all Dcps. As shown in Figure 8, Arg^{64} is part of a crescent of positive charge in *L. rhamnosus* Dcp not found in AcpP. The conserved Trp^{67} plays an important role in positioning helix II′, which in turn determines the orientation of Arg^{64} and creates one side of the cleft between helix II and the II−II′ loop (Figure 8). This cleft may also interact with the poly(Gro-P) moiety. Thus, on the basis of the results described in this paper, it is hypothesized that this region may constitute a part of the putative binding site for LTA in D-alanyl-Dcp.

The ACP family contains a variety of functionally specialized carrier proteins in addition to those involved in fatty acid biosynthesis. The best example of this specialization is found in the rhizobia (*54*). The genes encoding four ACPs have apparently diverged to ensure necessary functional specificity. In the case of *B. subtilis* (*55*), Dcp is encoded by *dltC* in the *dlt* operon, a chromosome location distinctly different from that of the gene encoding the carrier protein involved in fatty acid biosynthesis. Dcp not only binds to Dcl but also recognizes the LTA acceptor site [poly(Gro-P)], as well as DltD. The three-dimensional structure of apo-Dcp will allow the further definition of these specificity determinants for targeting this protein with its activated D-alanine in the assembly of membrane-associated D-alanyl-LTA.

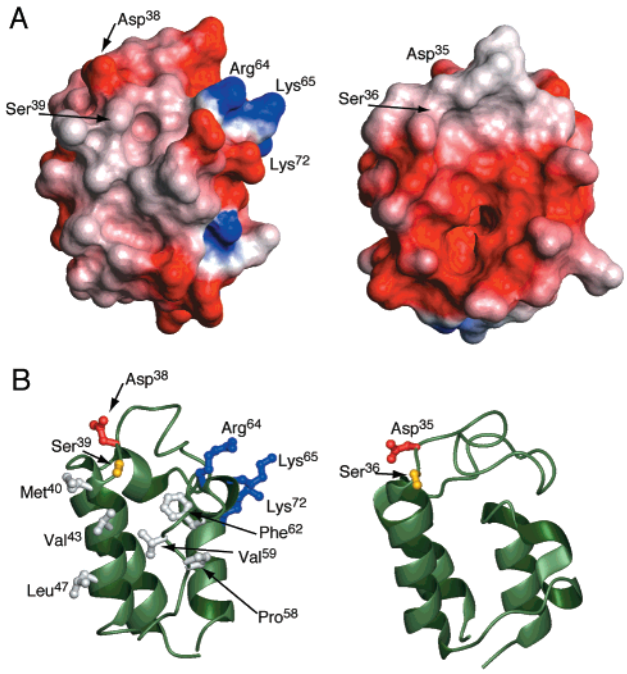

FIGURE 8: Putative poly(Gro-P) binding site of apo-Dcp. (A) Surface representations, colored according to electrostatic potential, are shown for apo-Dcp (left) and AcpP (right). Structures are oriented as in panels B and C of Figure 7 but with an additional 90° rotation about the vertical axis. Locations of the conserved Asp^{38} and Ser^{39} side chains are indicated (Asp^{35} and Ser^{36} in AcpP) as well as the cluster of basic residues proximal to the phosphopantetheine attachment site of apo-Dcp (Arg^{64}, Lys^{65}, and Lys^{72}). (B) Ribbon diagrams of apo-Dcp (left) and AcpP (right) in the same orientations as in panel A. Side chains are shown and labeled as in panel A (acidic residues in red, basic residues in blue, and active site serines in gold), with the addition of residues Met^{40}, Val^{43}, Leu^{47}, Pro^{58}, Val^{59}, and Phe^{62} of the hydrophobic cleft (white).

The importance of the D-alanyl carrier protein (Dcp) in the physiology of the Gram-positive organism is apparent from the many characterized *dlt* mutants which result in a deficiency of D-alanine esters in LTA (*56*−*63*). Insertional inactivation of any one of the four genes in the *dlt* operon has provided a variety of novel phenotypes. The inability of *dlt* mutants to synthesize the carrier molecule, the link between Dcl and the acceptor LTA, emphasizes the importance of understanding the functional and structural features of this protein.

ACKNOWLEDGMENT

We gratefully acknowledge the assistance of Dr. Ed Mooberry and other members of the NMRFAM staff. We are also grateful to Drs. Ruby I. MacDonald and Brian K. Shoichet for discussions and generous help with these

experiments. In addition, we thank Dr. Michael P. Heaton for many discussions and comments on the manuscript.

REFERENCES

1. Fischer, W. (1990) in *Handbook of lipid research: glycolipids, phospholipids, and sulfoglycolipids* (Kates, M., Ed.) pp 123−234, Plenum Publishing Corp., New York.
2. Heaton, M. P., and Neuhaus, F. C. (1992) *J. Bacteriol. 174*, 4707−4717.
3. Debabov, D. V., Heaton, M. P., Zhang, Q., Stewart, K. D., Lambalot, R. H., and Neuhaus, F. C. (1996) *J. Bacteriol. 178*, 3869−3876.
4. Heaton, M. P., and Neuhaus, F. C. (1994) *J. Bacteriol. 176*, 681−690.
5. Glaser, P., Kunst, F., Arnaud, M., Coudart, M. P., Gonzales, W., Hullo, M. F., Ionescu, M., Lubochinsky, B., Marcelino, L., Moszer, I., Presecan, E., Santana, M., Schneider, E., Schweizer, J., Vertes, A., Rapoport, G., and Danchin, A. (1993) *Mol. Microbiol. 10*, 371−384.
6. Perego, M., Glaser, P., Minutello, A., Strauch, M. A., Leopold, K., and Fischer, W. (1995) *J. Biol. Chem. 270*, 15598−15606.
7. Debabov, D. V., Kiriukhin, M. Y., and Neuhaus, F. C. (2000) *J. Bacteriol. 182*, 2855−2864.
8. Holak, T. A., Kearsley, S. K., Kim, Y., and Prestegard, J. H. (1988) *Biochemistry 27*, 6135−6142.
9. Holak, T. A., Nilges, M., Prestegard, J. H., Gronenborn, A. M., and Clore, G. M. (1988) *Eur. J. Biochem. 175*, 9−15.
10. Kim, Y., and Prestegard, J. H. (1990) *Proteins 8*, 377−385.
11. Crump, M. P., Crosby, J., Dempsey, C. E., Parkinson, J. A., Murray, M., Hopwood, D. A., and Simpson, T. J. (1997) *Biochemistry 36*, 6000−6008.
12. Weber, T., Baumgartner, R., Renner, C., Marahiel, M. A., and Holak, T. A. (2000) *Struct. Folding Des. 8*, 407−418.
13. Andrec, M., Hill, R. B., and Prestegard, J. H. (1995) *Protein Sci. 4*, 983−993.
14. Rawlings, M., and Cronan, J. E., Jr. (1992) *J. Biol. Chem. 267*, 5751−5754.
15. Sambrook, J., Fritsch, E. F., and Maniatis, T. (1989) *Molecular cloning: a laboratory manual*, 2nd ed., Cold Spring Harbor Laboratory Press, Plainview, NY.
16. Sturtevant, J. M. (1987) *Annu. Rev. Phys. Chem. 38*, 463−468.
17. Warren, W. S., Richter, W., Andreotti, A. H., and Farmer, B. T. (1993) *Science 262*, 2005−2009.
18. Zijl, P. C. M. V., Johnson, M. O. N., Mori, S., and Hurd, R. E. (1995) *J. Magn. Reson., Ser. A 113*, 256−270.
19. Kay, L. E., Xu, G. Y., and Yamazaki, T. (1994) *J. Magn. Reson., Ser. A 109*, 129−133.
20. Marion, D., and Wüthrich, K. (1983) *Biochem. Biophys. Res. Commun. 113*, 967−974.
21. Zhang, O., Kay, L. E., Olivier, J. P., and Forman-Kay, J. D. (1994) *J. Biomol. NMR 4*, 845−858.
22. Ikura, M., and Bax, A. (1992) *J. Am. Chem. Soc. 114*, 2433−2440.
23. McCoy, M. A., and Mueller, L. (1992) *J. Am. Chem. Soc. 114*, 2108−2112.
24. Muhandiram, D. R., and Kay, L. E. (1994) *J. Magn. Reson., Ser. B 103*, 203−216.
25. Wittekind, M., and Mueller, L. (1993) *J. Magn. Reson., Ser. B 101*, 201−205.
26. Kay, L. E., Xu, G.-Y., Singer, A. U., Muhandiram, D. R., and Forman-Kay, J. D. (1993) *J. Magn. Reson., Ser. B 101*, 333−337.
27. Grzesiek, S., Anglister, J., and Bax, A. (1993) *J. Magn. Reson., Ser. B 101*, 114−119.
28. Grzesiek, S., and Bax, A. (1992) *J. Magn. Reson. 96*, 432−440.
29. Bazzo, R., Cicero, D. O., and Barbato, G. (1995) *J. Magn. Reson., Ser. B 107*, 189−191.
30. Powers, R., Gronenborn, A. M., Clore, G. M., and Bax, A. (1991) *J. Magn. Reson. 94*, 209−213.
31. Mori, S., Abeygunawardana, C., Johnson, M. O., and van Zijl, P. C. M. (1995) *J. Magn. Reson., Ser. B 105*, 94−98.
32. Kuboniwa, H., Grzesiek, S., Delaglio, F., and Bax, A. (1994) *J. Biomol. NMR 4*, 871−878.
33. Vuister, G. W., and Bax, A. (1993) *J. Am. Chem. Soc. 115*, 7772−7777.
34. Archer, S. J., Ikura, M., Torchia, D. A., and Bax, A. (1991) *J. Magn. Reson. 95*, 636−641.
35. Santoro, J., and King, G. C. (1992) *J. Magn. Reson. 97*, 202−207.
36. Delaglio, F., Grzesiek, S., Vuister, G. W., Zhu, G., Pfeifer, J., and Bax, A. (1995) *J. Biomol. NMR 6*, 277−293.
37. Wishart, D. S., Bigam, C. G., Yao, J., Abildgaard, F., Dyson, H. J., Oldfield, E., Markley, J. L., and Sykes, B. D. (1995) *J. Biomol. NMR 6*, 135−140.
38. Bartels, C., Xia, T.-H., Billeter, M., Güntert, P., and Wüthrich, K. (1995) *J. Biomol. NMR 5*, 1−10.
39. Wishart, D. S., Bigam, C. G., Holm, A., Hodges, R. S., and Sykes, B. D. (1995) *J. Biomol. NMR 5*, 67−81.
40. Wishart, D. S., and Sykes, B. D. (1994) *J. Biomol. NMR 4*, 171−180.
41. Güntert, P., Mumenthaler, C., and Wüthrich, K. (1997) *J. Mol. Biol. 273*, 283−298.
42. Koradi, R., Billeter, M., and Wüthrich, K. (1996) *J. Mol. Graphics 14*, 51−55.
43. Laskowski, R. A., Rullmannn, J. A., MacArthur, M. W., Kaptein, R., and Thornton, J. M. (1996) *J. Biomol. NMR 8*, 477−486.
44. Horvath, L. A., Sturtevant, J. M., and Prestegard, J. H. (1994) *Protein Sci. 3*, 103−108.
45. Frederick, A. F., Kay, L. E., and Prestegard, J. H. (1988) *FEBS Lett. 238*, 43−48.
46. Schulz, H. (1975) *J. Biol. Chem. 250*, 2299−2304.
47. Tener, D. M., and Mayo, K. H. (1990) *Eur. J. Biochem. 189*, 559−565.
48. Privalov, P. L. (1980) *Pure Appl. Chem. 52*, 479−497.
49. Ghose, R., Geiger, O., and Prestegard, J. H. (1996) *FEBS Lett. 388*, 66−72.
50. Ritsema, T., Gehring, A. M., Stuitje, A. R., van der Drift, K. M. G. M., Dandal, I., Lambalot, R. H., Walsh, C. T., Thomas-Oates, J. E., Lugtenberg, B. J. J., and Spaink, H. P. (1998) *Mol. Gen. Genet. 257*, 641−648.
51. Kim, Y., and Prestegard, J. H. (1989) *Biochemistry 28*, 8792−8797.
52. Neuhaus, F. C., Heaton, M. P., Debabov, D. V., and Zhang, Q. (1996) *Microb. Drug Resist. 2*, 77−84.
53. Kiriukhin, M. Y., and Neuhaus, F. C. (2001) *J. Bacteriol. 183*, 2051−2058.
54. López-Lara, I. M., and Geiger, O. (2000) *Microbiology 146*, 839−849.
55. Morbidoni, H. R., de Mendoza, D., and Cronan, J. E., Jr. (1996) *J. Bacteriol. 178*, 4794−4800.
56. Boyd, D. A., Cvitkovitch, D. G., Bleiweis, A. S., Kiriukhin, M. Y., Debabov, D. V., Neuhaus, F. C., and Hamilton, I. R. (2000) *J. Bacteriol. 182*, 6055−6065.
57. Hyyrylainen, H. L., Vitikainen, M., Thwaite, J., Wu, H., Sarvas, M., Harwood, C. R., Kontinen, V. P., and Stephenson, K. (2000) *J. Biol. Chem. 275*, 26696−26703.
58. Peschel, A., Otto, M., Jack, R. W., Kalbacher, H., Jung, G., and Götz, F. (1999) *J. Biol. Chem. 274*, 8405−8410.
59. Clemans, D. L., Kolenbrander, P. E., Debabov, D. V., Zhang, Q., Lunsford, R. D., Sakone, H., Whittaker, C. J., Heaton, M. P., and Neuhaus, F. C. (1999) *Infect. Immun. 67*, 2464−2474.
60. Wecke, J., Perego, M., and Fischer, W. (1996) *Microb. Drug Resist. 2*, 123−129.
61. Duwat, P., Cochu, A., Ehrlich, S. D., and Gruss, A. (1997) *J. Bacteriol. 179*, 4473−4479.
62. Peschel, A., Vuong, C., Otto, M., and Götz, F. (2000) *Antimicrob. Agents Chemother. 44*, 2845−2847.
63. Spatafora, G. A., Sheets, M., June, R., Luyimbazi, D., Howard, K., Hulbert, R., Barnard, D., el Janne, M., and Hudson, M. C. (1999) *J. Bacteriol. 181*, 2363−2372.

BI010355A